Ab initio calculations on the defect structure of β-Ga_2O_3

T. Zacherle,[1,*] P. C. Schmidt,[2] and M. Martin[1]

[1]*Institute of Physical Chemistry, RWTH-Aachen University and JARA-FIT, 52056 Aachen, Germany*

[2]*Eduard-Zintl-Institute of Inorganic and Physical Chemistry, TU Darmstadt, 64287 Darmstadt, Germany*

(Received 12 March 2013; published 21 June 2013)

The intrinsic point defects of β-Ga_2O_3 are investigated using density functional theory. We have chosen two different exchange-correlation potentials: the generalized gradient approximation (GGA) and a hybrid potential (HSE06). Defect formation energies were determined taking into account finite-size effects. Schottky, anti-Frenkel, and Frenkel energies have been extracted for $T = 0$ K. We calculate formation entropies for an oxygen and a gallium vacancy and determine the Gibbs energy of Schottky disorder. Furthermore, we investigate the defect concentrations as a function of the oxygen partial pressure. The obtained purely intrinsic defect concentrations for charged defects are very small and result in a pO_2 dependence of the electron concentration of $[e'] \sim pO_2^{-1/6}$, whereas experimentally $[e'] \sim pO_2^{-1/4}$ is found. So we assume that, experimentally, a small unintentional donor doping is unavoidable. A small extrinsic donor concentration $[D^{\cdot}] = 10^{18}$ cm^{-3} (10 ppm) changes the electron concentration to $[e'] \sim pO_2^{-1/4}$ and gives an activation energy of the conductivity σ of 1.7 eV in good agreement to experimental values. So we propose as majority disorder $3[V_{Ga}'''] = [D^{\cdot}]$ with electrons being minority defects.

DOI: 10.1103/PhysRevB.87.235206 PACS number(s): 61.72.Bb, 61.72.J−, 63.20.−e, 72.80.Jc

I. INTRODUCTION

Monoclinic β-Ga_2O_3 is an n-type semiconductor with a wide band gap of 4.9 eV.[1] It has raised considerable interest in the last years due to its possible application as a deep UV transparent conducting oxide (TCO) material.[1,2] Gallium oxide can be produced in various nanostructures, e.g., nanowires[3] and nanoribbons,[4] and its nonstoichiometric amorphous phase shows memristive switching[5] and an abrupt increase of its conductivity upon heating due to local recrystallization.[6] β-Ga_2O_3 is already used in gas sensors with a characteristic pO_2 dependence of its electrical conductivity of $\sigma \sim pO_2^{-1/4}$.[7,8] The activation energy of the conductivity is reported to vary between 1.3 and 2.1 eV,[9,10] although there is also a measured activation energy of a single crystal with 3.3 eV[10]. The influence of donor (Zr, Ti) and acceptor (Mg) dopants on the conductivity[9,11] has been investigated experimentally and an inrease (decrease) of σ upon donor (acceptor) doping has been found. The luminescence behavior of β-Ga_2O_3 with broad emissions in UV, blue, and green[12] can also be altered by dopants such as Si[13] and N.[14] Especially Si has been identified as a common unintentional dopant in nominally pure gallium oxide samples.[9,15,16] There are no reports of p-type bulk phase Ga_2O_3 as the solubility of acceptor dopants is very small,[17] only for N-doped nanowires p-type behavior has been observed.[18]

Despite intense research in the last years, the question of the defect structure of gallium oxide is still not settled, although it is crucial for the understanding of the properties of the material and tailoring them to specifications needed for applications. Many different defect models have been proposed, varying from dominant oxygen vacancies $V_O^{\cdot}$ to gallium interstitials $Ga_i^{\cdot\cdot\cdot}$.[8,9] Both assumptions give the experimentally observed pO_2 dependence of the conductivity. However, dominating donor dopants (compensated, e.g., by gallium vacancies) with electrons being minority defects yields the same pO_2 dependence. It is the aim of this paper to study the defect structure by first-principles calculations and to give a consistent defect model, which can reproduce the main experimental results.

Various theoretical studies have been devoted to the bulk material.[19–25] Theoretical investigations of defects in β-Ga_2O_3 have for a long time been limited to empirical potentials, where oxygen vacancies have been identified as the defects with the lowest formation energies.[26] Recently, calculations on oxygen vacancies and donor impurities[27] and gallium vacancies[28] have been reported using density functional theory (DFT) with hybrid functionals. It was shown that the oxygen vacancies have deep donor states and hydrogen and silicon might easily be incorporated into the material. In addition, it was found that defect complexes of hydrogen atoms and gallium vacancies have low formation energies. Including these complexes in a defect model with unintentional donor doping results in a dependence of $\sigma \sim pO_2^{-1/4}$ as found experimentally. But the pO_2 dependence with slope $-1/4$ also holds at high temperatures (e.g., 1000 °C) where the gallium vacancy-hydrogen complexes are not believed to be stable. We will show in this paper that defect complexes are not needed to explain the main experimental findings. We present formation energies for all intrinsic point defects in gallium oxide. A special focus of this study will be the calculation of experimentally accessible quantities like the Schottky energy and defect concentrations. We find that it is essential to carefully correct for finite-size effects and to incorporate entropic contributions.

The paper is organized as follows. First, we introduce the theoretical framework in Sec. II. After describing computational details in Sec. III, we present formation energies for all simple point defects and investigate the occurring finite-size effects in Sec. IV. We also give values for the Frenkel, anti-Frenkel, and Schottky energies of our system (for $T = 0$ K). We calculate entropic contributions and the Gibbs energy of Schottky disorder, and the last part is concerned with defect concentrations, which can be extracted from the

calculated energies. Using these results, a defect model for β-Ga_2O_3 will be deduced. Lastly, we provide a short summary in Sec. V.

II. THEORY

In order to obtain full information about the defect structure of a system under usual experimental conditions, the Gibbs energies of defect formation $\Delta_f G^{p,T}$ for constant pressure p and temperature T have to be calculated:

$$\Delta_f G^{p,T} = \Delta_f E^{p,T} + p\Delta_f V^{p,T} - T\Delta_f S^{p,T}. \quad (1)$$

Here, $\Delta_f E^{p,T}$ denotes the formation energy, $\Delta_f V^{p,T}$ the formation volume, and $\Delta_f S^{p,T}$ the vibrational formation entropy, all at constant pressure p and temperature T. In *ab initio* studies, energies are usually computed at constant volume V and $T = 0$ K, and we have in good approximation[29–32] $\Delta_f H^{p,T} \approx \Delta_f E_0^V$, with the formation enthalpy at constant pressure $\Delta_f H^{p,T}$ and the static formation energy at constant volume and zero temperature $\Delta_f E_0^V$. This energy does not include the zero-point energy of the lattice vibrations.[31] So we will use the equation

$$\Delta_f G^{p,T} = \Delta_f E_0^V - T\Delta_f S^{p,T} \quad (2)$$

for our study. The first term $\Delta_f E_0^V$, which we will simply denote as formation energy $\Delta_f E$ in the remainder of this paper, can be calculated, e.g., for an oxygen vacancy $V_O^{\cdot\cdot}$, according to the well established formula[33–35]

$$\Delta_f E = E_{tot}(V_O^{\cdot\cdot}) - E_{tot}(\text{bulk}) + \mu_O + 2(E_{VBM} + E_{Fermi}) + E_{corr}(V_O^{\cdot\cdot}), \quad (3)$$

where $E_{tot}(V_O^{\cdot\cdot})$ is the total energy of the defective super cell and $E_{tot}(\text{bulk})$ is the total energy of the bulk cell. E_{VBM} is the energy of the valence band maximum (VBM) defined as $E_{VBM} = E_{tot}(q = 0) - E_{tot}(q = +1)$, where $E_{tot}(q = 0 \text{ or } +1)$ is the total energy for the neutral bulk or a super cell with one electron less.[36] E_{Fermi} is the Fermi level, which is set to zero at E_{VBM} and can vary from 0 to the energy of the optical band gap. $E_{corr}(V_O^{\cdot\cdot})$ denotes the energy correction due to finite-size effects (image charge and elastic effects). μ_O is the chemical potential of oxygen in a reservoir, which is a variable limited by the required phase stability of β-Ga_2O_3. We take the O_2 molecule (oxygen-rich condition) and the Ga metal (oxygen-poor condition) as limiting phases. Combining the expressions $\mu_O < 1/2\mu_{O_2} = 1/2E_{tot}(O_2)$; $\mu_{Ga} < \mu_{Ga}^{Ga-metal} = E_{tot}(Ga)$; $2\mu_{Ga} + 3\mu_O = \mu_{Ga_2O_3} = E_{tot}(Ga_2O_3)$ and the formation energy of the compound $\Delta_f E^{Ga_2O_3} = E_{tot}(Ga_2O_3) - 2\mu_{Ga}^{Ga-metal} - 3/2\mu_{O_2}$ one gets the range of μ_O, the chemical potential of oxygen in gallium oxide:

$$1/2\mu_{O_2} + 1/3\Delta_f E^{Ga_2O_3} < \mu_O < 1/2\mu_{O_2}. \quad (4)$$

The total energies (per formula unit) are here taken as a first approximation for the chemical potentials (corresponds to $T = 0$ K). We will follow this usual approach for the presentation of our energies, but extend our analysis to $T > 0$ K for the defect concentrations.

The second term on the right-hand side of Eq. (2) can be large for high temperatures[37] and so the effect of formation entropies $\Delta_f S^{p,T}$, which are essentially due to the change in frequencies of the lattice vibrations upon introduction of a defect, has to be considered as well. In our constant volume calculations, we obtain $\Delta_f S^{V,T}$ and for gallium vacancies, it can be written as[37]

$$\Delta_f S^{V,T}(V_{Ga}''') = S_{vib}(V_{Ga}''') - S_{vib}(\text{bulk}) + S_{Ga}, \quad (5)$$

where $S_{vib}(V_{Ga}''')$ and $S_{vib}(\text{bulk})$ are the vibrational entropy of the defective cell and bulk cell respectively and S_{Ga} is a partial vibrational entropy. This last term is important in order to rescale $S_{vib}(V_{Ga}''')$ and $S_{vib}(\text{bulk})$ to the same number of vibration modes. We can employ the well known connection between formation entropies at constant volumes and constant pressures (in our case $p = 0$ bar):[37–39]

$$\Delta_f S^{p,T} = \Delta_f S^{V,T} + \alpha B_T \Delta V_{rel}^{p,T}. \quad (6)$$

Here, α is the lattice expansion coefficient, B_T is the isothermal bulk modulus, and $\Delta V_{rel}^{p,T}$ is the relaxation volume of the defect. We will approximate this last quantity by its value at zero temperature and denote it by ΔV_{rel}, where $\Delta V_{rel} = V(\text{defect}) - V(\text{bulk})$ is simply obtained by performing a relaxation of the defective super cell to zero pressure to get $V(\text{defect})$ and subtracting the bulk volume $V(\text{bulk})$. The calculation of the temperature dependent relaxation volume would entail the calculation of formation entropies for different volumes of the defective cell,[32] which is computationally very demanding and beyond the scope of this study. So we obtain the following formula for our Gibbs free energies of formation:

$$\Delta_f G^{p,T} = \Delta_f E - T(\Delta_f S^{V,T} + \alpha B_T \Delta V_{rel}). \quad (7)$$

The obtained energies and Gibbs free energies of formation will be used to calculate defect concentrations. For example, in the strong dilution limit the concentration of gallium vacancies $[V_{Ga}''']$ can be written as

$$[V_{Ga}'''] = c_{Ga}\exp\left(-\frac{\Delta_f G^{p,T}}{k_B T}\right), \quad (8)$$

where c_{Ga} denotes the concentration of available gallium lattice sites. We compute the electron and hole concentration by integrating over the electronic density of states of the bulk system. The Fermi level for a fixed chemical potential of oxygen (or, equivalently, oxygen partial pressure pO_2) can then be determined by imposing charge neutrality.[34,40]

III. COMPUTATIONAL DETAILS

All DFT calculations in this study have been carried out using the Vienna *ab initio* simulation package VASP[41] and the projector augmented wave method PAW.[42,43] The $3d$, $4s$, and $4p$ electrons of gallium and the $2s$ and $2p$ electrons of oxygen are treated as valence electrons. For reasons outlined below, we used two different exchange-correlation potentials V_{xc}. We employ the PBE functional[44] within the generalized gradient approximnation (GGA) in order to be able to investigate the finite size scaling of the defect formation energies. In this context, cells of up to 360 atoms are computed. Mainly because it is known that GGA predicts a value for the optical band gap, which is approximately only half of the experimental one, we also used an orbital dependent hybrid functional. We have chosen the so-called HSE06 functional[45] with a fixed screening parameter of 0.2 $Å^{-1}$. The amount of exact exchange is set to 0.3 such that the calculated band gap is

in good agreement with the experimental value. As the hybrid functional is computationally very demanding we are restricted to a cell size of 80 atoms. Combining the results for the two different functionals, we will obtain band gap and finite-size corrected formation energies. For both the GGA and HSE06 formation energy calculations, a Monkhorst-Pack mesh[46] was employed for the k-point sampling. In the GGA case, the distance of the k points in the reciprocal lattice was less than 0.3 $Å^{-1}$ for all chosen supercells, in the HSE06 case a k-point distance of 0.5 $Å^{-1}$ was set during relaxation, and in a last run, the total energy of the converged configuration was recalculated with a finer k mesh with a maximal k-point distance of 0.3 $Å^{-1}$. Gaussian smearing with a smearing width of 0.1 eV was applied. All local relaxations of the ions were carried out at constant volume until the forces were less than 0.01 eV $Å^{-1}$. The energy cutoff was set to 500 eV and all calculations were spin polarized. For the calculation of the phonon frequencies, we use the so-called supercell method[47] and the GGA functional. We relax the bulk or the defective cell (120 atoms) at constant volume with the same k-point sampling as described above until the forces on the ions are less than 0.0001 eV $Å^{-1}$. The computation of the dynamical matrix is performed using displacements of 0.02 Å for both bulk and defective cell.

IV. RESULTS AND DISCUSSION

A. Bulk

The theoretically predicted lattice constants, band gap, and formation energy of β-Ga_2O_3 are listed in Table I for both the GGA and the HSE06 calculations together with literature data and experimental results. We adjusted the amount of exact exchange for the HSE06 calculations (0.3) in order to have good agreement of theoretical and experimental band gap. Our lattice parameters and energies agree well with other theoretical studies,[22,27] the slight differences to the HSE06 results from Ref. 27 can be explained by the fact that the amount of exact exchange chosen in this study (0.3) is smaller than in the literature (0.35). Overall, the HSE06 values are closer to experiment than the GGA data. In particular, the HSE06 formation energy of the compound is in better agreement to experiment as the O_2-binding energy (the experimental value is −5.2 eV) is better described by the hybrid functional (−5.0 eV) than the GGA functional (−6.0 eV).[48] The calculation of the vibrational frequencies yields a dispersion without imaginary frequencies. By computing the lattice vibrations of β-Ga_2O_3 for five different volumes of the unit cell and fitting the data to a Birch-Murnaghan equation of state,[49,50] we obtain the lattice expansion coefficient α and the isothermal bulk modulus B_T in quasiharmonic approximation. Comparison of these quantities to GGA data from the literature yields excellent agreement.

TABLE I. Lattice parameters, optical band gap, and formation energy of β-Ga_2O_3; listed are the GGA and HSE06 results of this work and literature data.

	GGA	GGA	HSE06	HSE06	Exp.
a (Å)	12.446	12.438[a]	12.253	12.25[b]	12.214[c]
b (Å)	3.083	3.084[a]	3.034	3.05[b]	3.037[c]
c (Å)	5.876	5.877[a]	5.789	5.84[b]	5.798[c]
β (deg)	103.70	103.71[a]	103.80	103.9[b]	103.83[c]
E_{gap} (eV)	2.0	–	4.7	4.83[b]	4.9[d]
$\Delta_f E^{Ga_2O_3}$ (eV)	−9.3	–	−10.3	−10.4[b]	−11.3[e]

[a]Reference 22.
[b]Reference 27.
[c]Reference 51.
[d]Reference 1.
[e]Reference 52.

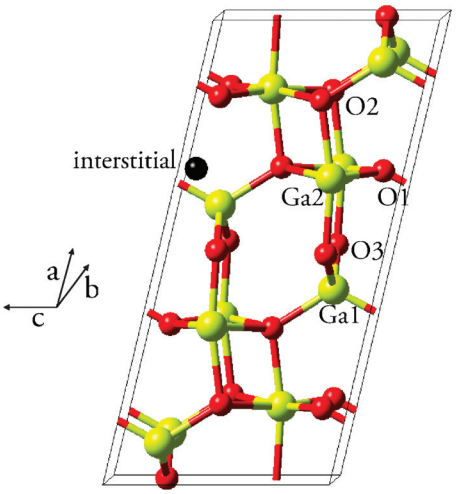

FIG. 1. (Color online) Monoclinic structure ($C2/m$) of β-Ga_2O_3. There are two different gallium and three different oxygen positions. The position before relaxation for O and Ga interstitials is indicated by the black sphere.

B. Defect formation energies

1. *Characterization of the defects*

The point defects differ in type, site and charge. In Fig. 1, we have displayed the possible defect sites in β-Ga_2O_3. As can be seen, a large number of different point defects has to be considered because of the low monoclinic symmetry of the compound ($C2/m$). There are two different lattice sites for gallium, Ga2 being octahedrally and Ga1 tetrahedrally coordinated by oxygen, and three different positions for oxygen. Therefore two different gallium vacancies and three different oxygen vacancies have to be considered. Furthermore, the most favorable interstitial sites have to be identified. As there is no obvious interstitial position in the system, many configurations have to be checked: up to seven different interstitial sites have been calculated. We found a low-energy configuration for gallium interstitials Ga_i and oxygen interstitials O_i. The position for both in units of the lattice vectors of the primitive cell before relaxation is the same (0.683, 0.0, 0.917), see Fig. 1. After the relaxation, the configurations differ strongly for the different charge states. In the case of $Ga_i^{\cdot}$, the local relaxation is small. However, $Ga_i^{\cdot\cdot}$ and $Ga_i^{\cdot\cdot\cdot}$ are moving neighboring ions from their bulk position into an interstitial position creating a double-interstitial-vacancy complex. For O_i, the changes in position due to the different charge of the ion are not so pronounced.

Another important point is that the localization of the electrons has to be checked. For the different vacancies no

problems arise, i.e., all charge states can be prepared, but in the case of the gallium interstitials, e.g., $Ga_i^{\cdot\cdot\cdot}$ cannot be prepared with GGA: the additional electron does not localize at the corresponding gallium atom but it is fully delocalized. So the actually prepared defect is $Ga_i^{\cdot\cdot\cdot} + e'(CB)$, i.e., a fully charged gallium ion and an electron in the conduction band (CB). In contrast, the defect $Ga_i^{\cdot\cdot}$ can be calculated without problems using HSE06. For the neutral gallium interstitial $Ga_i^{\times}$, the highest occupied state is delocalized for both functionals, so the actually calculated defects in the supercell are $Ga_i^{\cdot} + e'(CB)$. This shows that it is very important to check the localization of the electrons and to see whether the expected charge state has been successfully prepared or not. The localization of the defect electrons also plays an important role in the corrections of the so called finite size effects, which are considered next.

2. Finite-size scaling

The energy values gained from the band structure calculation cannot be used directly to describe the formation energy of isolated defects. Instead, these values have to be extrapolated to energy values for infinitely large supercells.

In a first step, the calculations have been performed with the GGA functional in order to obtain defect formation energies for different cell sizes. We have chosen supercells with 80 ($1 \times 2 \times 2$), 120 ($1 \times 3 \times 2$), 160 ($1 \times 4 \times 2$), and 240 ($1 \times 4 \times 3$) atoms. For special defects, for which the expected scaling has not yet been achieved, additional cells with 300 ($1 \times 5 \times 3$) and 360 ($1 \times 6 \times 3$) atoms are used. Figure 2 shows the results of these calculations for differently charged gallium vacancies V_{Ga2}. Because of the slowly decaying Coulomb interactions in the solid, image charge interactions are present in the energies even for the large cells.[53–55] As the leading term of the image charge interaction scales with $1/L$ (monopole term), we have plotted the uncorrected energy values as a function of $1/L$, where L is the average distance of the defect to its periodic image (see the right-hand side of Fig. 2). Due to the $1/L$ scaling, it is difficult to extrapolate to infinite dilution, as the energy axis is far from the calculated data points. Including image charge corrections, using the method proposed by Freysoldt *et al.*[56] and a calculated value of the dielectric constant of $\varepsilon_{GGA} = 12.7$, which is determined by means of density functional perturbation theory (DFPT) as the trace of the dielectric tensor (static electronic *plus* ionic contribution), results in the data plotted on the left-hand side of Fig. 2. There is still a slight size dependence on L for the following reason. Besides the electrostatic finite-size effects, there are also elastic finite size effects originating in different relaxations for different cell volumes. This contribution scales with $1/N_{Atom}$ or, equivalently, with $1/L^3$, where N_{Atom} is the number of atoms in the supercell.[38] We see from Fig. 2 that one gets indeed the expected $1/L^3$ scaling if the electrostatic corrections are included in the energy values. As this scaling moves the energy values for the large cells very close to the energy axis, extrapolation to infinite dilution is much more accurate. The procedure works well, although there is some deviation from the $1/L^3$ scaling for smaller cell sizes, which can be due to higher orders in elastic interactions. Oba *et al.*[57] have used a slightly different procedure for the extrapolation of GGA formation energies to infinite dilution, but we found that both procedures give very similar results. The average error of the linear extrapolation is smaller than 0.05 eV. As the computational cost for HSE06 calculations is very high, it is currently not feasible to carry out calculations of supercells with much more than 100 atoms within acceptable computation times. A full and explicit finite-size scaling is thus not possible for HSE06. Therefore we added the elastic corrections of the GGA energies to the energies of Freysoldt corrected HSE06 calculations (for the dielectric constant, we take the experimental value[58] of 10). Oba *et al.*[57] have used the same strategy to take the finite-size dependence of GGA energies and use it as an approximate correction for the finite-size effects in HSE06 energies. They have shown that this method yields band gap corrected and finite-size corrected formation energies. We will use these energies to calculate defect concentrations in Sec. IV D.

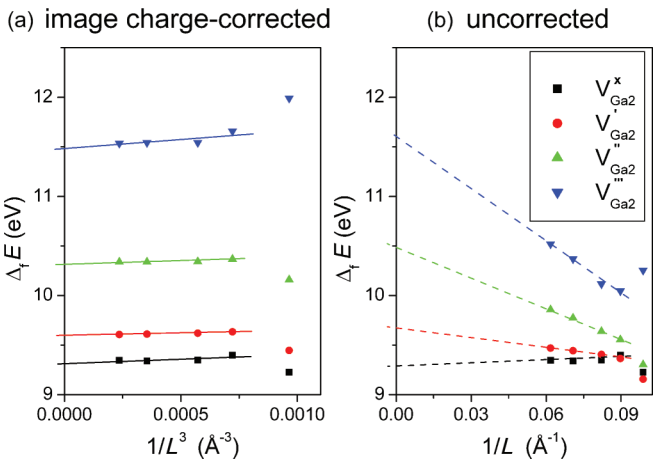

FIG. 2. (Color online) GGA formation energies of the gallium vacancies V_{Ga2} as a function of the average distance of defects L. In (a) electrostatic finite-size effects are included in the energy values. The cell size dependence is only due to elastic effects and the extrapolated values correspond to formation energies for infinite dilution of the defects. In (b), uncorrected energies are shown. The cell size dependence for the charged defects is mainly due to the monopole term in the image charge interaction.

3. Comparison GGA versus HSE06

(a) Formation energies of single point defects. The extrapolated values of the defect formation energies are listed in Table II for the two different potentials GGA and HSE06. The results are given for $E_{Fermi} = 0$ and for oxygen-poor conditions. We see that the GGA energies show the same trends as the HSE06 energies but the absolute values differ significantly. There is the general trend that positively charged defects have lower and negatively charged defects higher formation energies for HSE06 than for GGA. In addition, the energy differences (GGA versus HSE06) for the neutral defects are small compared to those of the charged defects. Ágoston *et al.*[59] attribute the lower $\Delta_f E$(HSE06) of oxygen vacancies $V_O^{\cdot\cdot}$ in TCO materials to reduced self-interaction and larger absolute values of the relaxation energy ΔE^{rel}. ΔE^{rel} is defined by separating the total formation energy $\Delta_f E$ into two parts, the energy to place the defect in the otherwise unchanged

TABLE II. Formation energies $\Delta_f E$ of the different point defects in β-Ga_2O_3. All energies are corrected for image charge and elastic effects (except the one marked with *, which is only image charge corrected) and correspond to energies for infinite dilution of the defects. O-poor conditions and $E_{\text{Fermi}} = 0$ are chosen.

Defect type	GGA $\Delta_f E$ (eV)	HSE06 $\Delta_f E$ (eV)	Defect type	GGA $\Delta_f E$ (eV)	HSE06 $\Delta_f E$ (eV)
$V_{O1}^{\times}$	1.15	1.37	$V_{Ga1}^{\times}$	9.03	9.84
$V_{O1}^{\cdot}$	−0.36	−1.41	$V_{Ga1}^{\prime}$	9.50	11.87
$V_{O1}^{\cdot\cdot}$	−2.25	−4.60	$V_{Ga1}^{\prime\prime}$	10.43	14.14
$V_{O2}^{\times}$	1.34	1.60	$V_{Ga1}^{\prime\prime\prime}$	11.97	16.91
$V_{O2}^{\cdot}$	−0.20	−1.25	$V_{Ga2}^{\times}$	9.31	10.91
$V_{O2}^{\cdot\cdot}$	−2.42	−4.76	$V_{Ga2}^{\prime}$	9.60	12.18
$V_{O3}^{\times}$	0.63	0.82	$V_{Ga2}^{\prime\prime}$	10.32	13.87
$V_{O3}^{\cdot}$	−0.10	−1.14	$V_{Ga2}^{\prime\prime\prime}$	11.47	16.30
$V_{O3}^{\cdot\cdot}$	−1.63	−3.74	$Ga_i^{\cdot}$	1.59	1.25
$O_i^{\times}$	6.48	7.22	$Ga_i^{\cdot\cdot}$	. . .	−2.50*
$O_i^{\prime}$	7.40	9.35	$Ga_i^{\cdot\cdot\cdot}$	−2.80	−6.35
$O_i^{\prime\prime}$	9.10	12.41			

lattice, ΔE^{lat}, and the energy gain by the local relaxation of the lattice, ΔE^{rel}. We found larger $|\Delta E^{\text{rel}}|$ for both, negative and positive defects. For $V_{O2}^{\cdot\cdot}$, we get $\Delta E^{\text{rel}}(\text{GGA}) = -2.7$ eV versus $\Delta E^{\text{rel}}(\text{HSE06}) = -3.7$ eV and for $V_{Ga2}^{\prime\prime\prime}$, $\Delta E^{\text{rel}}(\text{GGA}) = -2.7$ eV versus $\Delta E^{\text{rel}}(\text{HSE06}) = -3.5$ eV. Therefore the observation that positively charged defects have lower and negatively charged defects have higher formation energies for HSE06 than for GGA cannot be explained by relaxation effects. As a consequence, the reduced self-interaction for HSE06 has to play an important role.

The absolute energy values of the VBM cannot be compared for the different functionals as the energy scale is in general different. Nevertheless, the formation energies can be compared, as well as the contributions for the different functionals. There is a decrease of E_{VBM} of the bulk cell [$E_{\text{VBM}}(\text{GGA}) = 2.04eV$ versus $E_{\text{VBM}}(\text{HSE06}) = 1.06$ eV], which enters into Eq. (3) with a minus sign for negatively and a plus sign for positively charged defects. For example, for $V_{Ga2}^{\prime\prime\prime}$ the term $-3E_{\text{VBM}}$ is -6.12 eV for GGA but only -3.18 eV for HSE06, whereas for $V_{O2}^{\cdot\cdot}$, $+2E_{\text{VBM}}$ is $+4.08$ eV for GGA and $+2.12$ eV for HSE06. So the difference between $E_{\text{VBM}}(\text{GGA})$ and $E_{\text{VBM}}(\text{HSE06})$ is the main reason for the trend discussed here and consistent with the reduced self-interaction in HSE06 energies.

The defect formation energies have to be considered as a function of two variables, the chemical potential of oxygen and the Fermi energy, see Eq. (3). For oxygen-poor and oxygen-rich conditions, the energies are plotted against the Fermi-level in Figs. 3 and 4. The curves are always given for the charge states of lowest energy and the kinks in the plots denote changes in the charge state. One can see that the oxygen vacancy shows a negative U behavior like it has been observed for other TCO materials.[59] For oxygen-poor conditions, the oxygen vacancies are the defects with lowest formation energy, for oxygen-rich conditions, the gallium vacancies have low formation energies for high Fermi levels, which corresponds to donor doping. The interstitial defects have always high formation energies, except for $Ga_i^{\cdot\cdot\cdot}$ for very low Fermi energies. As pointed out above, the GGA and

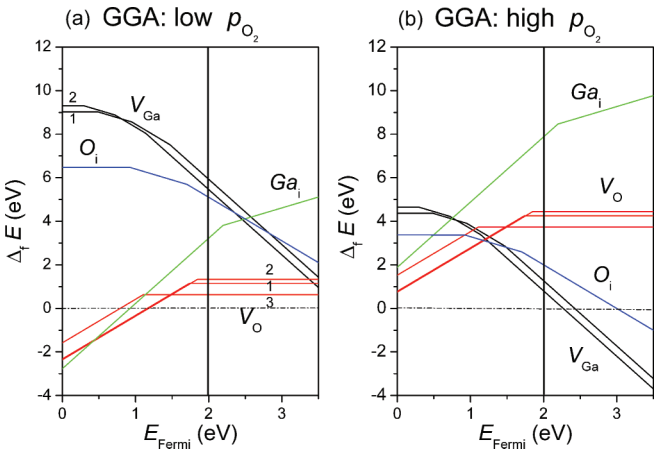

FIG. 3. (Color online) GGA formation energies of point defects in β-Ga_2O_3 plotted against the Fermi energy for (a) oxygen-poor and (b) oxygen-rich conditions. For V_{Ga}, the two different vacancies are denoted 1 (V_{Ga1}) and 2(V_{Ga2}). Analogous notation is used for the three oxygen vacancies. The straight vertical line shows the calculated position of the conduction band minimum.

HSE06 results display the same trends and the same ordering of energies. However, a major difference is that the transitions between two different charge states lie at higher Fermi levels for the hybrid functional. Comparing our hybrid functional energies with the ones obtained by Varley *et al.*,[27,28] we see differences for the $V_O^{\cdot\cdot}$ defects, which might be attributed to the differences in the amount of exact exchange (0.35 versus 0.30 in our study) and number of valence electrons. For the gallium vacancies, V_{Ga1} (tetrahedral site) is favorable for low E_{Fermi} and V_{Ga2} (octahedral site) for high E_{Fermi}, whereas in the study of Varley *et al.*, always V_{Ga1} is energetically lower. But they prepared a different kind of V_{Ga1}, which they derived from a transition state of the gallium vacancy migration, where one adjacent gallium atom changes to octahedral coordination.

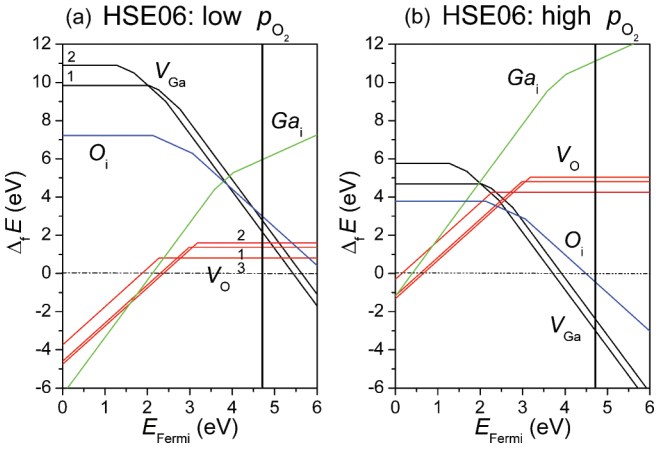

FIG. 4. (Color online) HSE06 formation energies of point defects in β-Ga_2O_3 plotted against the Fermi energy for (a) oxygen-poor and (b) oxygen-rich conditions. For V_{Ga}, the two different vacancies are denoted 1 (V_{Ga1}) and 2(V_{Ga2}). Analogous notation is used for the three oxygen vacancies. The straight vertical line shows the calculated position of the conduction band minimum.

TABLE III. Schottky, Frenkel, and anti-Frenkel energies per created defect for GGA and HSE06.

Reaction	Frenkel Eq. (9)	Anti-Frenkel Eq. (10)	Schottky Eq. (11)
GGA (eV)	4.33	3.34	3.14
HSE06 (eV)	4.98	3.83	3.66

(b) Schottky, Frenkel, and anti-Frenkel energies. From the combination of the individual defect formation energies for GGA and HSE06, we have also calculated Schottky, Frenkel, and anti-Frenkel energies for $T = 0$ K (all per created defect), see Table III. The corresponding reaction equations for Frenkel, anti-Frenkel, and Schottky disorders are

$$\mathrm{Ga}^{\times}_{\mathrm{Ga2}} \longleftrightarrow \mathrm{V}'''_{\mathrm{Ga2}} + \mathrm{Ga}^{\cdots}_{\mathrm{i}}, \tag{9}$$

$$\mathrm{O}^{\times}_{\mathrm{O2}} \longleftrightarrow \mathrm{V}^{\cdot\cdot}_{\mathrm{O2}} + \mathrm{O}''_{\mathrm{i}}, \tag{10}$$

$$2\mathrm{Ga}^{\times}_{\mathrm{Ga2}} + 3\mathrm{O}^{\times}_{\mathrm{O2}} \longleftrightarrow 2\mathrm{V}'''_{\mathrm{Ga2}} + 3\mathrm{V}^{\cdot\cdot}_{\mathrm{O2}} + \mathrm{Ga_2O_3}. \tag{11}$$

For both functionals, the anti-Frenkel and Schottky energies are close and distinctly lower than the Frenkel disorder energy. Taken into account our estimated error bars mentioned in Sec. IV B 2, we can only state that either Schottky or anti-Frenkel disorder is dominant—within the approximation of using zero-temperature energies calculated at constant volume, which are reported to be close to the enthalpy at constant pressure also for higher temperatures (see Fig. 3 in Ref. 32 for the case of anti-Frenkel disorder in In_2O_3). Comparing Tables II and III, we see that the differences in the defect reaction energies for the different functionals is smaller than the differences of the formation energies of single defects. This is due to the cancellation of errors for the combined defects. We have seen above that positively charged defects have lower formation energies and negatively charged ones higher formation energies for HSE06 than for GGA. This is the reason why the sum of both, e.g., $\Delta_\mathrm{f}E(\mathrm{V}^{\cdot\cdot}_{\mathrm{O2}})$ and $\Delta_\mathrm{f}E(\mathrm{V}'''_{\mathrm{Ga2}})$ for GGA tends to be close to the HSE06 value despite the rather large differences in formation energies for the single defects. This applies to all the above-mentioned defect reaction energies as they all are sums of formation energies of positively *and* negatively charged defects.

Summarizing the results of the energies of the different defect disorders we can state that the values obtained with HSE06 are more accurate due to the correct description of the band gap, but our results indicate as well that for the determination of the prevailing disorder it is sufficient to calculate the computationally much cheaper GGA energies, as a systematic error cancellation tends to restore the qualitative correct ordering of the energies.

C. Entropic contributions

1. Formation entropies of single point defects

The lattice vibrations contribute to the Gibbs energy of formation through the change in vibrational entropy, i.e., the term $-T\,\Delta_\mathrm{f}S^{p,T}$ [see Eqs. (1) and (6)]. This contribution can become important for high temperatures, which will be outlined in this section.

TABLE IV. ΔV_rel and $\alpha B_\mathrm{T}\Delta V_\mathrm{rel}$ (for $T = 1273$ K) for chosen defects in gallium oxide.

	$\mathrm{V}^{\cdot\cdot}_{\mathrm{O2}}$	$\mathrm{V}^{\cdot}_{\mathrm{O2}}$	$\mathrm{V}^{\times}_{\mathrm{O2}}$	$\mathrm{V}'''_{\mathrm{Ga2}}$	$\mathrm{O}''_{\mathrm{i}}$	$\mathrm{Ga}^{\cdots}_{\mathrm{i}}$
ΔV_rel (Å^3)	−12.64	−7.20	−1.93	31.38	32.03	−11.24
$\alpha B_\mathrm{T}\Delta_\mathrm{f}V$ (k_B)	−3.8	−2.2	−0.6	9.5	9.7	−3.4

All defect entropies were calculated for just one cell volume (the equilibrium volume of the perfect cell at $T = 0$ K), as already mentioned in Sec. II. Before we discuss our results concerning the phonon dispersions of the defective cells, we first focus on the second term on the right-hand side of Eq. (6). In Table IV, we give values for ΔV_rel and $\alpha B_\mathrm{T}\Delta V_\mathrm{rel}$ (for $T = 1273$ K) for some chosen intrinsic defects. We can see the following trends. The negatively charged defects like $\mathrm{V}'''_{\mathrm{Ga2}}$ and $\mathrm{O}''_{\mathrm{i}}$ have large positive relaxation volumes, whereas the positively charged defects like $\mathrm{V}^{\cdot\cdot}_{\mathrm{O2}}$ and $\mathrm{Ga}^{\cdots}_{\mathrm{i}}$ have negative and smaller relaxation volumes. This is also found by Àgoston *et al.*[37] for In_2O_3, indicating that this might be a rather general behavior. The entropic contributions for $T = 1273$ K amount to over 9 k_B for $\mathrm{O}''_{\mathrm{i}}$ and $\mathrm{V}'''_{\mathrm{Ga2}}$ and lie around -3 k_B for $\mathrm{V}^{\cdot\cdot}_{\mathrm{O2}}$ and $\mathrm{Ga}^{\cdots}_{\mathrm{i}}$.

The formation entropy at constant volume $\Delta_\mathrm{f}S^{V,T}$ is calculated according to Eq. (5).[37] As the calculations of the entropies of the defective cells are computationally very demanding with up to 500 calculations for one phonon dispersion due to the low symmetry of the system, we only calculated the gallium vacancy $\mathrm{V}'''_{\mathrm{Ga2}}$ and the oxygen vacancy $\mathrm{V}^{\cdot\cdot}_{\mathrm{O2}}$. We chose the first one because it is the most important charged defect for high Fermi levels (i.e., donor doping) (see Fig. 4) and the last one as it is the dominating defect for Fermi levels in the middle of the band gap (see also Fig. 4). As will be shown later these defects are important to understand donor doped ($\mathrm{V}'''_{\mathrm{Ga2}}$) and pure ($\mathrm{V}^{\cdot\cdot}_{\mathrm{O2}}$) gallium oxide, and we will use their formation entropies as reasonable estimates for the formation entropies of the other vacancy defects for our calculation of the defect concentrations.

Because of the low symmetry of the system, we could not avoid for the chosen defective supercells (119 atoms), limited by computing time, a dispersion with some imaginary frequencies. The phonon dispersion of the gallium vacancy $\mathrm{V}'''_{\mathrm{Ga2}}$ is displayed in Fig. 5. One acoustic branch is imaginary around the Γ point, which is indicated by negative frequencies in Fig. 5. In total, 0.06% of the volume of the first Brillouin zone is contaminated by imaginary frequencies. As has been shown by Grabowski *et al.*[60] for the metals Pd and Pb, these kind of imaginary frequencies are not indications of lattice instabilites but they are due to the finite size of the simulation cell. By increasing the cell size, they arrive at phonon dispersions without imaginary frequencies. As this approach is computationally too demanding for our low-symmetry system, we perform a correction in order to extract reliable entropy values. As the contributions of the imaginary frequencies are set to zero for the calculation of the entropies, we effectively have less degrees of freedom, which contribute to the calculated thermodynamic quantities. To account for this, we slightly modify Eq. (5) by rescaling the bulk entropy to the same effective number of degrees of freedom as the

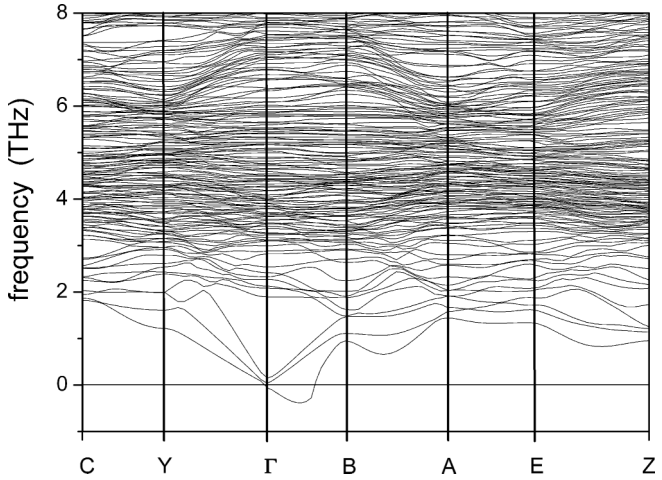

FIG. 5. Excerpt of the phonon dispersion for the defect V'''_{Ga2} with some some imaginary frequencies around the Γ point, which are displayed here as negative frequencies.

defective entropy:

$$\Delta_f S^{V,T}(V'''_{Ga}) = S_{vib}(V'''_{Ga}) - \eta[S_{vib}(\text{bulk}) + S_{Ga}], \quad (12)$$

with $\eta = 1 - 0.0006 = 0.9994$. For the oxygen vacancy $V^{\cdot\cdot}_{O2}$, we perform the same correction procedure as we have 0.09% of the volume of the first Brillouin zone contaminated by imaginary frequencies. In Fig. 6, the calculated $\Delta_f S^{p,T}$ and $\Delta_f S^{V,T}$ are displayed for both vacancies as a function of temperature. It is found that for constant volume, the formation entropy stays essentially constant for $T > 300$ K, which has also been observed for different formation entropies in In_2O_3.[37] The stronger dependence of the constant pressure formation entropy on temperature is due to the term $\alpha B_T \Delta V_{rel}$, which of course is also temperature dependent. The contribution $-T\Delta_f S^{p,T}$ to the Gibbs free energy of formation is −1.61 eV (V'''_{Ga2}) and +0.25 eV ($V^{\cdot\cdot}_{O2}$) for $T = 1273$ K.

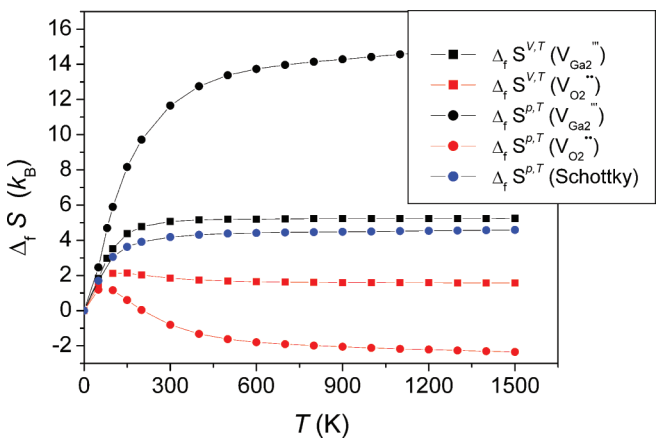

FIG. 6. (Color online) Defect formation entropies of V'''_{Ga2} and $V^{\cdot\cdot}_{O2}$ for constant volume $\Delta_f S^{V,T}$ and constant pressure $\Delta_f S^{p,T}$. In addition, the Schottky formation entropy (per created defect) for constant pressure is given.

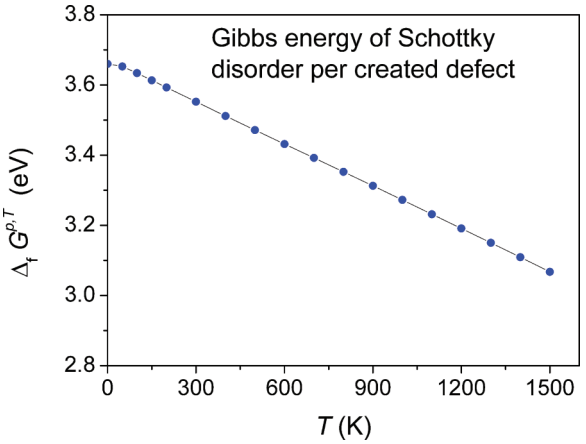

FIG. 7. (Color online) Temperature dependence of the Gibbs energy of Schottky disorder [see Eq. (11)].

2. *Gibbs energy of Schottky disorder*

As we have calculated the entropies of formation of the oxygen and gallium vacancies from the reaction given in Eq. (11), we can give values for the Gibbs energy of Schottky disorder in gallium oxide. The big advantage of Schottky, Frenkel, or anti-Frenkel Gibbs energies is that the external chemical potentials, which are major contributions and sources of error to the formation energies exactly cancel. So we obtain an energy, which does not depend on thermodynamic conditions and is considered as a general characteristic of the defect chemistry of a certain material.

The formation entropy $\Delta_f S^{p,T}$ of Schottky disorder is simply obtained by adding the formation entropies for the single defects in stoichiometric amounts and dividing the obtained value by the number of created defects. In Fig. 6, the temperature dependence of the corresponding entropy for Schottky disorder is shown: it is essentially constant above 300 K with a value of about 4.5 k_B. Adding the entropic contribution $-T\Delta_f S^{p,T}$ to the Schottky energy (see Table III) one obtains the Gibbs free energy of Schottky disorder, which is shown in Fig. 7. A linear decrease of the energy can be observed from 3.66 eV at zero temperature to about 3.1 eV for $T = 1500$ K.

D. Defect concentrations

It is shown in the previous section that entropic contributions to the Gibbs energies can become important. These contributions have to be taken into consideration for (i) the calculation of the stability limits of β-Ga_2O_3 and (ii) the computation of realistic defect concentrations. First, we consider the limiting phases.

The chemical potentials we used for the calculation of the formation energies, see Figs. 3 and 4, were constrained to lie within the stability field of β-Ga_2O_3, which is given by Eq. (4). Up to this point, the permitted range of chemical potentials was determined using the total energy values of the limiting phases: the O_2 gas and the Ga metal. Although this is common practice in the literature, these values are only valid for $T = 0$ K. As we want to extend our analysis of the defect properties of gallium oxide to the case of $T > 0$ K, we also have to include the temperature dependence of the

chemical potentials in our phase stability considerations. For this purpose, we follow the approach of Osorio-Guillén *et al.*[61] with two modifications. First, we take the $T = 0$ K total energy of the oxygen molecule $\frac{1}{2}E_{\mathrm{tot}}(O_2)$ to be approximately the enthalpy under reference conditions, i.e., temperature $T_0 = 298.15$ K and pressure $P_0 = 1$ bar. The remaining temperature and pressure dependence is taken from thermochemical tables,

$$\mu_O(T, pO_2) = \frac{1}{2}E_{\mathrm{tot}}(O_2) + \Delta\mu_O(T, P_0) + \frac{1}{2}k_B T \ln\left(\frac{pO_2}{P_0}\right), \tag{13}$$

with $\Delta\mu_O(T, P_0)$ being the change in chemical potential from the reference temperature T_0 to temperature $T > T_0$. We slightly generalize the approach proposed by Osorio-Guillén *et al.*[61] by also calculating μ_{Ga} and $\mu_{Ga_2O_3}$ in this manner, in order to get a reliable and coherent phase stability range for the different temperatures. So all chemical potentials, which are also major contributions to the formation energies [see Eq. (3)], are determined on the same footing. In this way, we can compute defect concentrations depending on partial pressures pO_2 and compare our results directly to experimental data.

Due to the fact that we do not have a full set of formation entropies and we want to avoid artificial trends by using entropies only for certain charge states, we take the constant volume formation entropies $\Delta_f S^{V,T}$ calculated for V'''_{Ga2} and $V^{\cdot\cdot}_{O2}$ as a reasonable (but untested) estimate for the formation entropies of all charge states of all corresponding vacancy types (gallium and oxygen). For all defects, i.e., vacancies *and* interstitials, we take into account the contribution $\alpha B_T \Delta V_{\mathrm{rel}}$. A further comment on the formation entropies is in place here. As we now include the full chemical potentials, e.g., μ_O from Eq. (13), in our formation energies, we must not correct the obtained entropies with an additional term like the partial entropy in Eqs. (5) and (12) for the calculation of our defect concentrations.

1. Pure β-Ga_2O_3

In Fig. 8, we display the defect concentrations of pure gallium oxide against the oxygen partial pressure for $T = 1273$ K. The calculated stability range is from $pO_2 = 1$ bar to $pO_2 \approx 10^{-16}$ bar. The lower boundary compares well with the experimental value[62] of 10^{-15} bar for $T = 1273$ K, which validates our modified approach for the calculation of the phase stability limits. The numerically determined Fermi energy varies from 2.48 eV (oxygen-rich conditions) to 3.14 eV (oxygen-poor conditions). There are two majority defects: electrons (dark yellow line) and oxygen vacancies (red straight and dotted lines). The electrons are charge compensated by doubly charged oxygen vacancies $V^{\cdot\cdot}_O$ (denoted by"••" in Fig. 8) over the whole pO_2 range, i.e., $[e'] = 2[V^{\cdot\cdot}_O]$. The neutral oxygen vacancies (denoted by "×" in Fig. 8) become more abundant than the doubly charged vacancies under oxygen poor conditions, but the charged vacancies still compensate the electrons, as is indicated by the dotted red lines. The singly charged oxygen vacancies $V^{\cdot}_O$ have lower concentrations than $V^{\cdot\cdot}_O$ over the whole pO_2 range. The stoichiometric point, i.e., $[e'] = [h^{\cdot}]$ would be at $pO_2 \approx 10^1$ bar, but as the mobility of electron holes in gallium oxide is much lower than the mobility of electrons,[25] even at high pO_2 no p-type conductivity in pure β-Ga_2O_3 can be expected. The pO_2 dependence of $[e']$ in Fig. 8 can easily be derived from the mass action law of the reaction:

$$O^{\times}_O \longleftrightarrow V^{\cdot\cdot}_O + 2e' + \tfrac{1}{2}O_2(\mathrm{gas}). \tag{14}$$

Using $[e'] = 2[V^{\cdot\cdot}_O]$ results in a pO_2 dependence of $[e'] \sim pO_2^{-1/6}$.

The calculated concentration can be converted to a electronic conductivity under the assumption of a pO_2-independent mobility of electrons. It follows that $\sigma \sim [e'] \sim pO_2^{-1/6}$ contrary to the experimental finding of $\sigma \sim pO_2^{-1/4}$. We conclude that unintentional dopants must play an important role to understand the conductivity behavior. This assumption is obvious because the obtained intrinsic defect concentrations for charged defects are very small, 10^{13}–10^{14} cm^{-3}. Therefore even a small amount of charged dopants will dominate the defect structure and the purely intrinsic regime is very unlikely to be observed experimentally.

2. Donor doped β-Ga_2O_3

There is increasing evidence in the literature—both theoretical[27,63] and experimental[15,16]—that unintentional donors like silicon are present in the material and might be the cause for the n-type conductivity in gallium oxide. We have shown in the previous section that purely intrinsic defect concentrations are so small that already minor amounts of impurities will completely dominate the defect structure. So now we investigate the effect of weak donor doping in β-Ga_2O_3.

In Fig. 9, we plot the defect concentrations of 10 ppm donor doped gallium oxide against the oxygen partial pressure for $T = 1273$ K. We chose an extrinsic donor concentration of 10 ppm (10^{18} cm^{-3}), because this value is an average of typical impurity concentrations given in the literature.[9,63] The

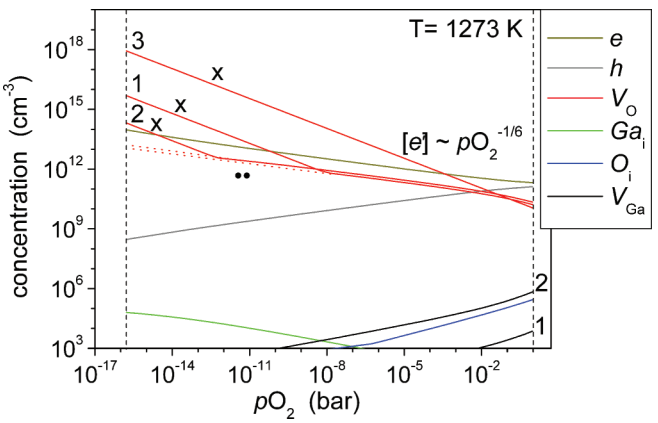

FIG. 8. (Color online) Defect concentrations of pure gallium oxide plotted against oxygen partial pressure pO_2 for $T = 1273$ K. The phase stability limits are indicated by the vertical dashed lines. Oxygen vacancies (red straight and dotted lines) compensate the electrons (dark yellow) for all pO_2, yielding a pO_2 dependence of the electron concentration with exponent $-1/6$. For low pO_2, the neutral oxygen vacancies ("×") become more abundant than the doubly charged vacancies ("••"), but the electrons are still compensated by the charged vacancies (dotted red lines). Numbers indicate the vacancy sites for V_{Ga} and V_O.

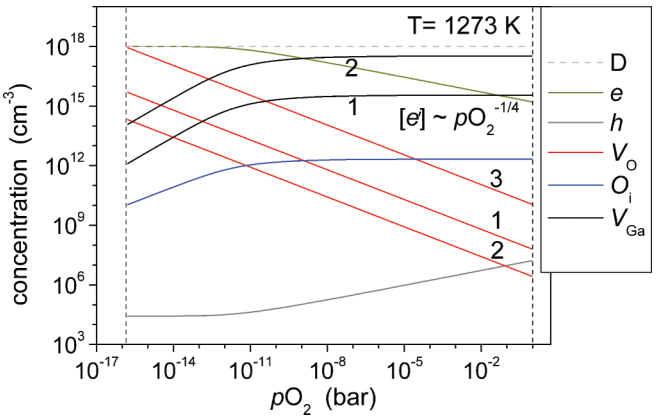

FIG. 9. (Color online) Defect concentrations of 10 ppm donor doped gallium oxide plotted against oxygen partial pressure pO_2 for $T = 1273$ K. The phase stability limits are indicated by the vertical dashed lines. Gallium vacancies V'''_{Ga2} (black line) compensate the donor (dashed grey line) in a large pO_2 range. The electrons are minority defects with $[e] \sim pO_2^{-1/4}$, as found experimentally. Numbers indicate the vacancy sites for V_{Ga} and V_O.

numerically determined Fermi energy varies from 3.47 eV (oxygen rich conditions) to 4.16 eV (oxygen poor conditions). Gallium vacancies V'''_{Ga2} (black line denoted by "2") compensate the donor (dashed grey line) in a large pO_2 range, i.e., $3[V'''_{Ga}] = [D^{\cdot}]$. The electrons become minority defects already for low pO_2 and the resulting pO_2 dependence of the electron concentration is $[e'] \sim pO_2^{-1/4}$, as found experimentally. Only at very low pO_2 the donor is compensated by electrons resulting in $[e'] \sim pO_2^{0}$. The oxygen vacancies (red lines) are neutral and their concentrations get high only for very low pO_2. From defect concentrations at different temperatures ($T =$ 973–1273 K, $pO_2 = 0.2$ bar), we determined an activation energy of the electron concentration of 1.10 eV. For 100-ppm donor concentration, we obtain a value of 1.08 eV, showing that this energy does not strongly depend on the dopant level. Taking the experimental value[10] of 0.6 eV for the activation energy of the electron mobility in gallium oxide, we arrive at an activation energy of the conductivity σ of 1.7 eV. This is in good agreement to most of the published experimental values, ranging from 1.3 to 2.1 eV for high temperatures.[9,10]

Experimentally[62] $[e'] \sim pO_2^{-1/4}$ is found down to a pO_2 of 10^{-15} bar for $T = 1273$ K. The reason why our simulations give the right exponent $-1/4$ only for $pO_2 > 10^{-11}$ bar might be due to the assumption that the relaxation volume $\Delta V_{rel}^{p,T}$ of the defects does not depend on temperature, which will be the case, in general. There are reports on increasing, e.g., anti-Frenkel formation volumes with increasing temperature.[32,64] This quantity is identical to the sum of the relaxation volumes of an oxygen vacancy and an oxygen interstitial and its temperature dependence shows that also the relaxation volumes of the individual defects will change with temperature. An increase of $\Delta V_{rel}^{p,T}$ for the gallium vacancies would lower their Gibbs energy of formation and therefore extend the range of $[e'] \sim pO_2^{-1/4}$ to lower pO_2 values.

V. CONCLUSION

We have calculated fully finite size corrected defect formation energies for all point defects in gallium oxide using the GGA and HSE06 functionals. Although there are rather larger quantitative differences for the different functionals, we showed that there is qualitative agreement in the ordering of the energies. We determined Schottky, Frenkel, and anti-Frenkel energies and saw that Schottky disorder has the lowest energy for both functionals, although the anti-Frenkel disorder is only slightly less favorable. We investigated the entropic contribution to the Gibbs free energy of formation for V'''_{Ga2} and $V^{\cdot\cdot}_{O2}$ and found a large formation entropy for the gallium vacancy of 14 k_B for high temperatures. With the calculated entropies, we were able to compute the Gibbs energy of Schottky disorder in gallium oxide and obtained a decrease from 3.7 eV at $T = 0$ K to 3.2 eV at $T = 1273$ K. Finally, we calculated defect concentrations and showed that the concentrations of charged defects in pure gallium oxide are very low (in agreement with measurements of the nonstoichiometry of gallium oxide by means of coulometric titration).[65] Therefore already small amounts of unintentional donors completely change the defect structure. With only 10 ppm of donor impurities, we could reproduce the experimental pO_2 dependence of the electron concentration with exponent $-1/4$ over a wide pO_2 range. In addition, we find an activation energy of the conductivity σ of 1.7 eV, which is in good agreement with experimental values. We propose the defect model $3[V'''_{Ga}] = [D^{\cdot}]$ with the electrons being minority defects.

ACKNOWLEDGMENTS

The authors gratefully acknowledge the computing time granted by the John von Neumann Institute for Computing (NIC) and provided on the supercomputer JUROPA at Jülich Supercomputing Centre (JSC). We thank Walter Wolf from Materials Design® and Masanobu Nakayama from Nagoya Institute of Technology for support and helpful discussion. Financial support by the SFB 917 "Nanoswitches" is also gratefully acknowledged.

*zacherle@pc.rwth-aachen.de

[1] M. Orita, H. Ohta, M. Hirano, and H. Hosono, Appl. Phys. Lett. **77**, 4166 (2000).

[2] N. Ueda, H. Hosono, R. Waseda, and H. Kawazoe, Appl. Phys. Lett. **70**, 3561 (1997).

[3] H. Zhang, Y. Kong, Y. Wang, X. Du, Z. Bai, J. Wang, D. Yu, Y. Ding, Q. Hang, and S. Feng, Solid State Commun. **109**, 677 (1999).

[4] Z. R. Dai, Z. W. Pan, and Z. L. Wang, J. Phys. Chem. B **106**, 902 (2002).

[5] X. Gao, Y. Xia, J. Ji, H. Xu, Y. Su, H. Li, C. Yang, H. Guo, J. Yin, and Z. Liu, Appl. Phys. Lett. **97**, 193501 (2010).

[6] L. Nagarajan, R. A. De Souza, D. Samuelis, I. Valov, A. Borger, J. Janek, K.-D. Becker, P. C. Schmidt, and M. Martin, Nat. Mater. **7**, 391 (2008).

[7]M. Fleischer and H. Meixner, Sens. Actuators B **4**, 437 (1991).
[8]T. Sasaki and K. Hijikata, Proc. Inst. Natl. Sci. Nihon Univ. **9**, 209 (1974).
[9]T. Harwig and J. Schoonman, J. Solid State Chem. **23**, 205 (1978).
[10]M. Fleischer and H. Meixner, J. Appl. Phys. **74**, 300 (1993).
[11]J. Frank, M. Fleischer, and H. Meixner, Sens. Actuators B **34**, 373 (1996).
[12]L. Binet and D. Gourier, J. Phys. Chem. Solids **59**, 1241 (1998).
[13]K. Shimamura, E. G. Villora, T. Ujiie, and K. Aoki, Appl. Phys. Lett. **92**, 201914 (2008).
[14]Y. Zhang, J. Yan, Q. Li, C. Qu, L. Zhang, and T. Li, Physica B: Condens. Mat. **406**, 3079 (2011).
[15]E. G. Villora, K. Shimamura, T. Ujiie, and K. Aoki, Appl. Phys. Lett. **92**, 202118 (2008).
[16]K. Iwaya, R. Shimizu, H. Aida, T. Hashizume, and T. Hitosugi, Appl. Phys. Lett. **98**, 142116 (2011).
[17]D. Roehrens, J. Brendt, D. Samuelis, and M. Martin, J. Solid State Chem. **183**, 532 (2010).
[18]L. Liu, M. Li, D. Yu, J. Zhang, H. Zhang, C. Qian, and Z. Yang, Appl. Phys. A **98**, 831 (2010).
[19]K. Yamaguchi, Solid State Commun. **131**, 739 (2004).
[20]H. He, M. A. Blanco, and R. Pandey, Appl. Phys. Lett. **88**, 261904 (2006).
[21]H. He, R. Orlando, M. A. Blanco, R. Pandey, E. Amzallag, I. Baraille, and M. Rérat, Phys. Rev. B **74**, 195123 (2006).
[22]S. Yoshioka, H. Hayashi, A. Kuwabara, F. Oba, K. Matsunaga, and I. Tanaka, J. Phys.: Condens. Matter **19**, 346211 (2007).
[23]B. Liu, M. Gu, and X. Liu, Appl. Phys. Lett. **91**, 172102 (2007).
[24]M. Mohamed, C. Janowitz, I. Unger, R. Manzke, Z. Galazka, R. Uecker, R. Fornari, J. R. Weber, J. B. Varley, and C. G. V. de Walle, Appl. Phys. Lett. **97**, 211903 (2010).
[25]J. B. Varley, A. Janotti, C. Franchini, and C. G. Van de Walle, Phys. Rev. B **85**, 081109 (2012).
[26]M. A. Blanco, M. B. Sahariah, H. Jiang, A. Costales, and R. Pandey, Phys. Rev. B **72**, 184103 (2005).
[27]J. B. Varley, J. R. Weber, A. Janotti, and C. G. Van de Walle, Appl. Phys. Lett. **97**, 142106 (2010).
[28]J. B. Varley, H. Peelaers, A. Janotti, and C. G. Van de Walle, J. Phys.: Condens. Matter **23**, 334212 (2011).
[29]M. J. Gillan, Philos. Mag. A **43**, 301 (1981).
[30]J. Harding, Physica B + C **131**, 13 (1985).
[31]M. B. Taylor, G. D. Barrera, N. L. Allan, T. H. K. Barron, and W. C. Mackrodt, Faraday Discuss. **106**, 377 (1997).
[32]A. Walsh, A. A. Sokol, and C. R. A. Catlow, Phys. Rev. B **83**, 224105 (2011).
[33]G. A. Baraff and M. Schlüter, Phys. Rev. Lett. **55**, 1327 (1985).
[34]S. B. Zhang and J. E. Northrup, Phys. Rev. Lett. **67**, 2339 (1991).
[35]C. G. Van de Walle and J. Neugebauer, J. Appl. Phys. **95**, 3851 (2004).
[36]C. Persson, Y.-J. Zhao, S. Lany, and A. Zunger, Phys. Rev. B **72**, 035211 (2005).
[37]P. Ágoston and K. Albe, Phys. Chem. Chem. Phys. **11**, 3226 (2009).
[38]Y. Mishin, M. R. Sorensen, and A. F. Voter, Philos. Mag., Part A **81**, 2591 (2001).
[39]C. R. A. Catlow, J. Corish, P. W. M. Jacobs, and A. B. Lidiard, J. Phys. C: Solid State **14**, L121 (1981).
[40]P. Erhart and K. Albe, J. Appl. Phys. **104**, 044315 (2008).
[41]G. Kresse and J. Furthmüller, Phys. Rev. B **54**, 11169 (1996).
[42]P. E. Blöchl, Phys. Rev. B **50**, 17953 (1994).
[43]G. Kresse and D. Joubert, Phys. Rev. B **59**, 1758 (1999).
[44]J. P. Perdew, K. Burke, and M. Ernzerhof, Phys. Rev. Lett. **77**, 3865 (1996).
[45]J. Heyd, G. E. Scuseria, and M. Ernzerhof, J. Chem. Phys. **118**, 8207 (2003).
[46]H. J. Monkhorst and J. D. Pack, Phys. Rev. B **13**, 5188 (1976).
[47]K. Parlinski, Z-. Q. Li, and Y. Kawazoe, Phys. Rev. Lett. **78**, 4063 (1997).
[48]L. Wang, T. Maxisch, and G. Ceder, Phys. Rev. B **73**, 195107 (2006).
[49]F. Birch, Phys. Rev. **71**, 809 (1947).
[50]F. Murnaghan, Am. J. Math. **59**, 235 (1937).
[51]J. Åhman, G. Svensson, and J. Albertsson, Acta Cryst. C **52**, 1336 (1996).
[52]I. Barin and G. Platzki, *Thermochemical Data of Pure Substances*, Bd. 1-2 (Wiley-VCH, Weinheim, 1995).
[53]M. Leslie and N. J. Gillan, J. Phys. C: Solid State **18**, 973 (1985).
[54]G. Makov and M. C. Payne, Phys. Rev. B **51**, 4014 (1995).
[55]S. Lany and A. Zunger, Phys. Rev. B **78**, 235104 (2008).
[56]C. Freysoldt, J. Neugebauer, and C. G. Van de Walle, Phys. Rev. Lett. **102**, 016402 (2009).
[57]F. Oba, A. Togo, I. Tanaka, J. Paier, and G. Kresse, Phys. Rev. B **77**, 245202 (2008).
[58]M. Passlack, N. E. J. Hunt, E. F. Schubert, G. J. Zydzik, M. Hong, J. P. Mannaerts, R. L. Opila, and R. J. Fischer, Appl. Phys. Lett. **64**, 2715 (1994).
[59]P. Ágoston, K. Albe, R. M. Nieminen, and M. J. Puska, Phys. Rev. Lett. **103**, 245501 (2009).
[60]B. Grabowski, T. Hickel, and J. Neugebauer, Phys. Rev. B **76**, 024309 (2007).
[61]J. Osorio-Guillén, S. Lany, S. V. Barabash, and A. Zunger, Phys. Rev. Lett. **96**, 107203 (2006).
[62]M. Fleischer, L. Höllbauer, E. Born, and H. Meixner, J. Am. Ceram. Soc. **80**, 2121 (1997).
[63]T. C. Lovejoy, R. Chen, X. Zheng, E. G. Villora, K. Shimamura, H. Yoshikawa, Y. Yamashita, S. Ueda, K. Kobayashi, S. T. Dunham, F. S. Ohuchi, and M. A. Olmstead, Appl. Phys. Lett. **100**, 181602 (2012).
[64]J. H. Harding, Phys. Rev. B **32**, 6861 (1985).
[65]H.-S. B. Kim, H.-I. Yoo, and M. Martin (unpublished).